Acetate formation on metals via CH_4 carboxylation by CO_2: A DFT study

Md. Saeedur Rahman and Ye Xu*

† *Cain Department of Chemical Engineering, Louisiana State University, Baton Rouge, Louisiana 70803, United States*

* Corresponding author. E-mail: yexu@lsu.edu.

Abstract

Density functional theory calculations have been performed to investigate CH_4 activation and coupling to CO_2 forming C_2 carboxylates such as acetate on the close-packed (111) or (0001) surfaces of ten late transition and coinage metals (Co, Ni, Cu, Ru, Rh, Pd, Ag, Ir, Pt, and Au). Consistent with the literature, the activation energy (E_a) for the initial C-H bond scission in CH_4 is mild, being ca. 1 eV or less on all but the coinage metals, of which Ag exhibits the highest E_a at 2.13 eV, followed by Au and Cu. E_a for the CH_3-CO_2 coupling step is 0.8 ~ 1.1 eV on Co, Ru, Rh, and Ag, 1.2 ~ 1.5 eV on Ni, Cu, Pd, and Ir, and 1.8 ~ 2.1 eV on Pt and Au. While the two E_a are comparable for several metals in terms of DFT total energies, free energy analysis indicates CH_3-CO_2 coupling to be much more rate-limiting than CH_4 activation. Overcoming it would require over 800 K even on the most active of the metals considered, Ru, which makes the formation of acetate not feasible on the monometallic metal surfaces. Instead, we propose that single atom alloys based on early transition metals doped into a host metal such as Ni(111) could be viable catalysts. The dopant sites serve to stabilize the transition state of C-C coupling while Ni sites continue to activate CH_4, thereby significantly lowering the required temperature for acetate formation.

Keywords

Carbon Dioxide; Methane; Carboxylation; Acetate; Alloy catalysis; DFT

1. Introduction

There has been tremendous research and commercial interest in the chemical transformation of two abundant C1 compounds, methane (CH_4) and carbon dioxide (CO_2), into value-added fuels and chemicals due to potential environmental and economic benefits [1]. Industrially, methane is primarily converted via steam reforming (SRM) to hydrogen and syngas at over 1000 K [2,3]. SRM requires significant energy input and has a large CO_2 footprint due to its strongly endothermic nature [4]:

$$CH_4 + H_2O \rightarrow CO + 3H_2 \qquad \Delta H^\circ_{298} = +206 \text{ kJ/mol}, \Delta G^\circ_{298} = +151 \text{ kJ/mol}$$

Another method to utilize CH_4 is to replace H_2O with CO_2 in what is termed dry reforming (DRM):

$$CH_4 + CO_2 \rightarrow 2CO + 2H_2 \qquad \Delta H^\circ_{298} = +247 \text{ kJ/mol}, \Delta G^\circ_{298} = +171 \text{ kJ/mol}$$

Like SRM, DRM is also strongly endothermic and requires over 800 K to achieve any significant equilibrium conversion [5]. DRM has seen limited commercial deployment where a concentrated CO_2 stream is available and where syngas with a $CO:H_2$ ratio different from what SRM produces is desired [6]. Syngas is the starting point for the production of a wide range of organic compounds.

Over the years, an alternate reaction pathway has been explored in which CH_4 and CO_2 react together to produce a specific compound, acetic acid, with more favorable overall thermodynamics than DRM:

$$CH_4 + CO_2 \rightarrow CH_3COOH \qquad \Delta H^\circ_{298} = +36 \text{ kJ/mol}, \Delta G^\circ_{298} = +71 \text{ kJ/mol}$$

Commercial production for acetic acid currently begins with methanol synthesis from syngas, followed by methanol carbonylation. Methane carboxylation by CO_2 (hereafter abbreviated as MCC) could reduce the number of process steps and separation and transportation needs.

The viability of MCC to acetic acid is contingent upon having a suitable catalyst that can actively and selectively catalyze the desired chemical transformation. A small body of research can be found in the literature on the performance of various catalysts for this reaction [7]. Several studies used a stepwise route or co-fed additional reactants (H_2, H_2O, or O_2) with CH_4 and CO_2 to circumvent the thermodynamic limitations [8–11]. Few studies have attempted directly reacting a mixture of only CH_4 and CO_2, with the highest stable rates of acetic acid formation reported to date being ca. 400 μmol $gcat^{-1}{\cdot}hr^{-1}$ at 500 ºC over alkali-promoted Cu-ZSM-5 [12,13]. Formic acid and methanol were often produced in significant quantities with acetic acid [8,13]. Spectroscopic evidence of surface acetate or acetic acid species was noted in some studies. Spivey and co-workers detected acetate species on Pd/carbon and Pt/alumina using DRIFTS when the catalysts were exposed to CH_4 and CO_2 at 400 ºC [14]. Chen and co-workers reported features attributable to bidentate acetate species using DRIFTS after exposing Fe/ZnO to CO_2 and CH_4 [15]. In these studies, the acetate features were much weaker than those of surface CO_x species. Shavi et al. captured methyl H and carbonyl C signals attributable to acetic acid in solid-state ^{13}C and ^{1}H NMR on montmorillonite-supported CeO_2-ZnO catalysts [13].

Fundamentally, unlike DRM, in which the forward reaction produces a greater number of molecules and is therefore favored by entropy and high temperature, the opposite is true for MCC, the ΔG° of which worsens with increasing temperature that would nonetheless be needed to overcome the high kinetic barrier for activating CH_4. Without involving additional chemical species, these constraints could be compensated for by simultaneously increasing temperature and pressure, a situation reminiscent of the Haber-Bosch process. Another possible way to circumvent thermodynamics is to aim for formation of surface acetate species as an intermediate

in an overall organic synthesis reaction that has more favorable thermodynamics than MCC to acetic acid. This was the idea behind the study by Spivey and co-workers in which acetylene was co-fed with CO_2 and CH_4 to form vinyl acetate [16].

Here we report a DFT based investigation of the carboxylation of CH_4 by CO_2 to C_2 carboxylates such as acetate on the close-packed surfaces of 3d (Co(0001), Ni(111), and Cu(111)), 4d (Ru(0001), Rh(111), Pd(111), and Ag(111)), and 5d (Ir(111), Pt(111), and Au(111)) metals, aiming to identify trends in CH_4 activation and C-C coupling activity across the common catalytic metals and to identify which metals may be best suited for catalyzing this partial reaction. Defect sites such as steps and corners are expected to be more active for CH_4 activation than the close-packed surfaces for each metal, which we will consider in a future study. Our results show that the energy of the transition states of the two steps scales closely with the adsorption energy of atomic C and O, respectively. When free energy is taken into account, CH_3-CO_2 coupling is much more rate-limiting than CH_4 activation on all the surfaces considered. Although acetate is concluded by previous density functional theory (DFT) studies to be the most stable state in MCC on many catalysts based on electronic energy [13,15,17], a lack of significant amounts of acetate species actually detected on catalysts corroborates either a rate-limiting C-C coupling step or an unfavorable free energy profile for acetate. It is concluded that the focus of catalyst engineering should be placed on promoting the latter step, for which a catalyst design strategy is proposed.

2. Methods

Periodic DFT calculations were performed using the Vienna Ab initio Simulation Package (VASP, version 5.4.4) [18] in the generalized gradient approximation (GGA-PBE [19]). Bloch's

projector augmented wave (PAW) method was used to treat the interactions between valence electrons and ionic cores [20,21]. The Kohn-Sham wave function was expanded in a plane wave basis set with a kinetic energy cutoff up to 400 eV. The electron occupancies were determined according to the Methfessel-Paxton scheme [22] with an energy smearing of 0.1 eV. Brillouin zone integration was performed using the Monkhorst-Pack method [23] on a Γ-centered 5×5×1 k-point grid. Each metal surface was simulated using a four-layer periodic slab with a p(3×3) supercell and ca. 15 Å vacuum space between neighboring images in the z direction. The atoms in the bottom two-layer of each slab were kept fixed at their bulk positions, whereas the top two layers were fully relaxed during optimization. All structures were optimized until each force component of each relaxed atom was less than 0.03 eV/Å. All calculations were non-spin-polarized except for Ni(111) and Co(0001). The optimized lattice constants for the ten metals were: Co, 2.492/4.024 Å; Ni, 3.518 Å; Cu, 3.633 Å; Ru, 2.726/4.302 Å; Rh, 3.824 Å; Pd, 3.939 Å; Ag, 4.188 Å; Ir, 3.872 Å; Pt, 3.971 Å; and Au, 4.157 Å.

The adsorption energy of adsorbate was calculated as $\Delta E_{ads} = E_{total} - E_{slab} - E_{gas}$, where E_{total} is the energy of the slab with adsorbates, E_{slab} is the energy of the clean slab without any adsorbate, and E_{gas} is the energy of the adsorbate molecule in a neutral state placed in the gas phase. Gas phase molecules were calculated in a simulation cell of 18×18×18 $Å^3$. Negative ΔE_{ads} values indicate exothermic chemisorption.

Transition states (TSs) were optimized using the dimer method [24] with a force convergence criterion of 0.01 eV/Å. For an elementary reaction step, the activation energy (E_a) was defined as the difference in total energy between the TS and the initial state (IS): $E_a = E_{TS} - E_{IS}$, and the reaction energy (ΔE_{rxn}) as the energetic difference between the final state (FS) and the IS: $\Delta E_{rxn} = E_{FS} - E_{IS}$. When the IS or FS involved multiple species, ΔE_{rxn} was calculated

based on those species at infinite separation. Vibrational frequencies were calculated using the harmonic oscillator approximation by diagonalizing the mass-weighted Hessian matrix. Each calculated TS was verified to have only one vibrational mode with a negative curvature in the direction of the bond breaking or formation.

The standard activation free energy was obtained by adding a correction term (δG_a) to the activation energy as defined above (E_a), which was computed as: $\delta G_a(T) = \delta G_{TS}(T) - \sum_i \delta G_{IS,i}(T,p)$, where the δG_i terms are free energy corrections for individual surface or gas phase species. δG_i for surface species (including TSs) was calculated in the harmonic limit, whereas δG_i for each gas phase species (CH_4 and CO_2) was calculated in the ideal gas limit at a pressure of 1 bar, using the Atomic Simulation Environment [25].

3. Results and discussion

3.1. CH_4 activation and coupling to CO_2

We begin by considering CH_4 dissociating into a methyl group (CH_3) and atomic H on the given metal surfaces. The adsorption of molecular CH_4 on close-packed transition metal surfaces is dominated by van der Waals interactions and is kinetically inconsequential [26,27]. The calculated E_a and ΔE_{rxn} for the initial C-H scission are reported in Table 1. Examples of the corresponding minimum-energy TS structures are shown in Figure 1.

Table 1. GGA-PBE calculated activation barrier (E_a, in eV), reaction energy (ΔE_{rxn}, in eV), and C-H distance at TS ($d_{C\text{-}H}$, in Å) for initial C-H scission in CH_4 on the ten metal surfaces.

Surface	E_a	ΔE_{rxn}	$d_{C\text{-}H}$	E_a (literature)
Co(0001)	1.02	0.00	1.588	1.16 [28], 1.08 [29]
Ni(111)	0.86	-0.04	1.586	0.95 [30], 0.93 [31]
Cu(111)	1.56	+0.75	1.773	1.56 [32], 1.54 [33]
Ru(0001)	0.74	-0.31	1.575	0.80 [32], 0.78 [34]
Rh(111)	0.69	+0.14	1.550	0.69 [35], 0.67 [32], 0.60 [36]
Pd(111)	0.71	+0.03	1.560	0.73 [37], 0.86 [32]
Ag(111)	2.13	+1.65	1.891	n/a
Ir(111)	0.81	+0.22	1.517	0.93 [38], 0.84 [39]
Pt(111)	0.77	+0.04	1.484	0.74 [40], 0.70 [41]
Au(111)	1.75	+1.16	1.715	1.78 [32]

E_a and ΔE_{rxn} are computed with respect to gas-phase CH_4. C-H bond distance in gas-phase CH_4 is 1.096 Å.

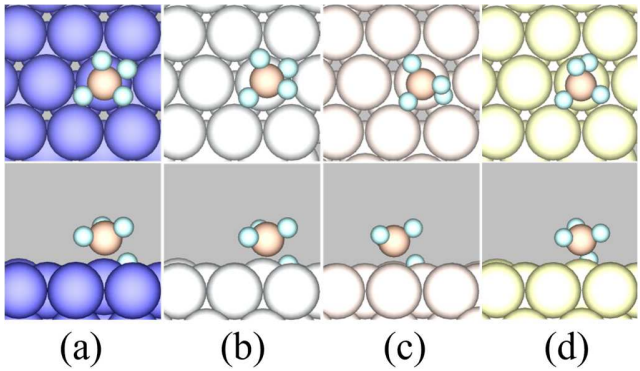

Figure 1. Top (top panels) and side (bottom panels) views of GGA-PBE optimized TS structures for C-H scission on (a) Co(0001); (b) Ni(111); (c) Ru(0001); and (d) Ir(111). Those on the remaining metals are shown in Figure S1. Color code: large spheres = metals; medium brown spheres = C; medium red spheres = O; small blue spheres = H.

The TSs of the initial C-H scission in CH_4 on the 3d metals (Co, Ni, and Cu) are similar, with the dissociating H atom located over a nearest threefold fcc hollow site. The H atom moves to a bridge site in the TS on the 4d (Ru, Rh, Pd, and Ag) and 5d (Ir, Pt, and Au) metals. The C-H distance in the TS is lengthened to 1.5~1.6 Å except on Cu, Ag, and Au, where it exceeds 1.7 Å. The calculated total-energy E_a is quite mild, being ca. 1 eV or less on all but the coinage metals, but as we will show below, the activation free barriers could be significantly higher. ΔE_{rxn} is strongly endothermic on the coinage metals but deviates only mildly from thermal neutrality on the other meals. Both E_a and ΔE_{rxn} considered, Ag(111) is the most passive among all the given metals toward CH_4 dissociative adsorption, followed by Au(111) and Cu(111). These results for catalytic CH_4 activation are generally in accord with previous DFT studies using comparable methods for the given metal surfaces [28,30,32,37,40,42,43].

The other key step in this reaction is the formation of a C-C bond between CH_3 and CO_2 to form a surface CH_3COO species. E_a and ΔE_{rxn} for the C-C coupling step are reported in Table

2, together with the various interatomic distances between the carbon, oxygen, and surface metal atoms in the TSs of this step. The snapshots of the TSs are shown in Figure 2. The TSs are slightly more stable when located on the fcc site on some metals and more stable on the hcp site on other metals, but the differences do not exceed 0.02 eV.

Table 2. GGA-PBE calculated activation barrier (E_a, in eV), reaction energy (ΔE_{rxn}, in eV), and various interatomic distances (d's, in Å) in the TS, for CH_3-CO_2 coupling on the ten metals surfaces.

Surface	E_a	ΔE_{rxn}	$d_{C1\text{-}C2}$	$d_{M3\text{-}C1}$	$d_{C2\text{-}O1}$	$d_{C2\text{-}O2}$	$d_{M1\text{-}O1}$	$d_{M2\text{-}O2}$
Co(0001)	1.12	-0.78	1.983	2.157	1.302	1.304	1.985	1.982
Ni(111)	1.22	-0.67	2.017	2.088	1.290	1.290	1.981	1.975
Cu(111)	1.34	-1.02	2.163	2.141	1.205	1.228	2.693	2.185
Ru(0001)	0.75	-0.93	1.941	2.322	1.316	1.318	2.086	2.083
Rh(111)	0.92	-0.88	1.924	2.253	1.297	1.298	2.122	2.120
Pd(111)	1.52	-0.37	2.015	2.226	1.264	1.269	2.227	2.194
Ag(111)	0.90	-1.21	2.228	2.368	1.208	1.209	2.657	2.626
Ir(111)	1.51	-0.67	1.877	2.330	1.309	1.312	2.129	2.120
Pt(111)	2.15	-0.04	1.936	2.288	1.279	1.284	2.201	2.182
Au(111)	1.76	-0.26	2.034	2.437	1.218	1.220	2.676	2.633

E_a and ΔE_{rxn} are computed with respect to gas-phase CO_2. C-O bond distance in gas-phase CO_2 is 1.177 Å. See Figure 2a for labeling of atoms.

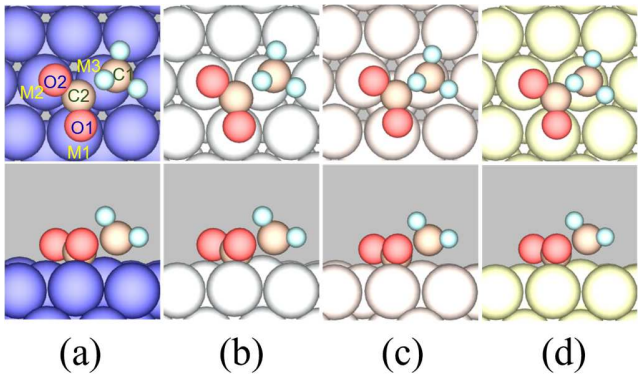

Figure 2. Top (top panels) and side (bottom panels) views of GGA-PBE optimized TS structures for CH_3-CO_2 coupling on (a) Co(0001); (b) Ni(111); (c) Ru(0001); (d) Ir(111). Those on the remaining metals are shown in Figure S2. Color code: large spheres = metal; medium brown spheres = C; medium red spheres = O; small blue spheres = H.

The C-C distance varies between 1.8~2.1 Å in the TS of the C-C coupling step ($d_{C1\text{-}C2}$). In the TS, the CO_2 moiety that inserts into the methyl-surface bond adopts a bent structure, which is an indicator that charge transfer has occurred that puts the CO_2 in a partially anionic state [44–48]. Both C-O bonds are considerably lengthened compared to gas-phase CO_2, and they are no longer equal in length. The O atom (O1) that is slightly closer to the C atom (C2) ($d_{C2\text{-}O1} < d_{C2\text{-}O2}$) is always slightly farther away from the metal atom underneath it than the other O atom (O2) ($d_{M1\text{-}O1} > d_{M2\text{-}O2}$). Both C-O distances are shorter on the coinage metals than on the rest of the metals, which reflects the weaker interaction between oxygen and the coinage metals.

The calculated E_a for the C-C coupling step are larger than those for the initial CH_4 activation step for several metals. It is ca. 0.8 ~ 1.1 eV on the Co, Ru, Rh, and Ag surfaces, higher (1.2 ~ 1.5 eV) on the Ni, Cu, Pd, and Ir surfaces, and the highest on Pt and Au surfaces at 1.8 ~ 2.1 eV. Overall, the mid transition metals are more active than the late ones for this step, with the 4d metals being more active than the 3d metals, followed by the 5d metals. These

trends are influenced by both C (for CH_3) and O (for the C-C coupling TS) descriptors, as can be seen below. The C-C coupling step is notably more exothermic than the initial CH_4 activation step on all the metal surfaces.

3.2. Analysis of the transition states of CH_4 activation and C-C coupling to CO_2

Wang et al. reported that the TS of C-H scission in CH_4 scales linearly not only with the energy of the dissociated products, but also with the adsorption energy of atomic C (ΔE_C) on metal surfaces [49]. This is confirmed by our study (Figure 3a). The interaction of this TS with the metal surfaces involves partial de-bonding of the methyl moiety from the top site of a surface metal atom and de-bonding of an H atom from the surface. Since ΔE_H also scales closely with ΔE_C [49], the sum of these two interactions produces a slope (0.38) that is somewhat larger than 0.26, the slope of how the adsorption energy of the methyl group (ΔE_{CH3}) alone scales with ΔE_C [50], and is in agreement with Wang et al. who reported a slope of ca. 0.35 on close-packed metal surfaces [49]. Incidentally, consistent with previous theoretical studies, atomic C is found to prefer the threefold fcc site on Cu(111) [51], Pt(111) [52], and Au(111) [53], while it prefers the threefold hcp site on Co(0001) [28], Ni(111) [54], Ru(0001) [55], Rh(111) [56], Pd(111) [57], and Ir(111) [58]. On the other hand, atomic O is found to prefer the fcc site on the (111) facet of all of the fcc metals considered (Ni, Cu, Rh, Pd, Ir, Pt, and Au) and the hcp site on the (0001) facet of Co and Ru, which is also consistent with the previous studies.

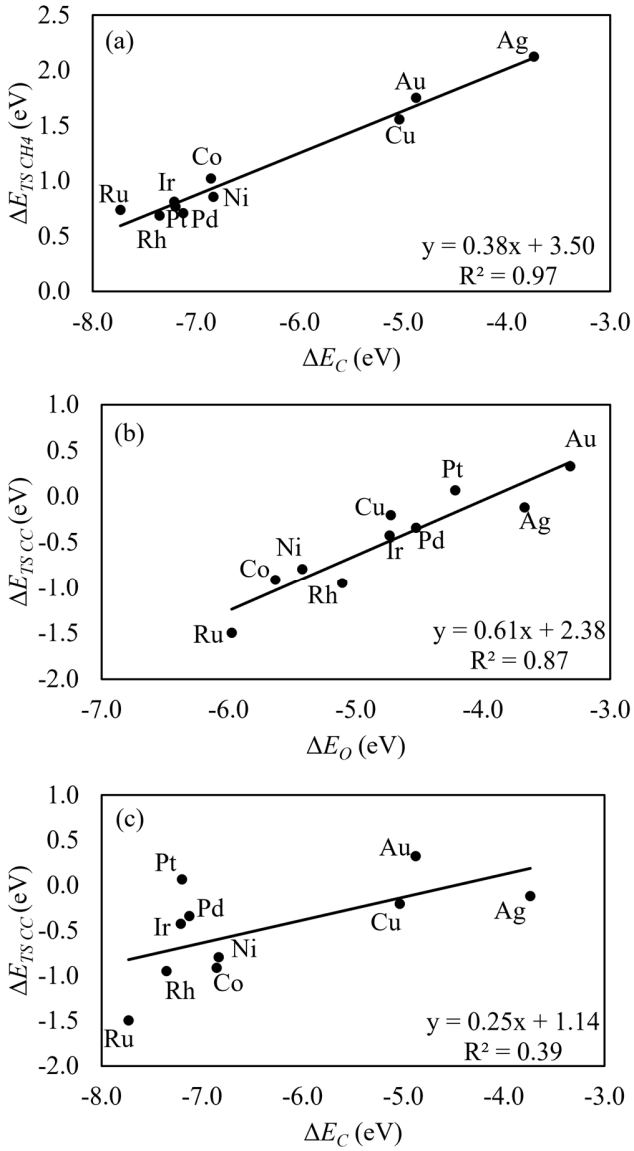

Figure 3. Adsorption energy of the TSs (ΔE_{TS}) of (a) CH_4 dissociation and CH_3-CO_2 coupling as a function of the adsorption energy (ΔE) of either (b) atomic C or (c) atomic O on the ten metal surfaces. ΔE_{TS} is calculated with respect to gas-phase CH_4 in (a) and to gas-phase neutral acetate group in (b, c).

What is less obvious is why ΔE_O is a better descriptor than ΔE_C for the energy of the TS of the C-C coupling step (compare Figure 3b,c), which formally involves bond formation

between two C atoms. To shed light on this phenomenon, we analyze the projected density of states (pDOS) for the TSs of the C-C coupling step. The pDOS of selected metal surfaces is shown in Figure 4. The pDOS plots for the remaining metal surfaces are included in Figure S3 in Supplementary Information.

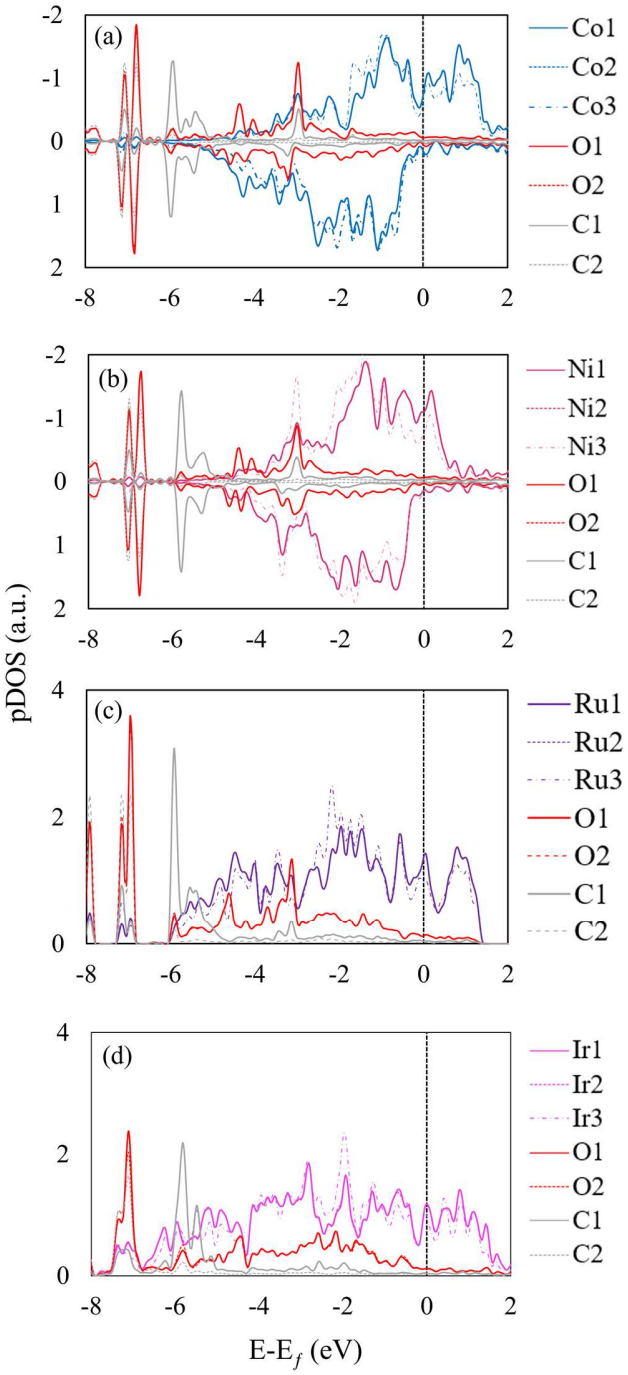

Figure 4. Projected density of state (pDOS) of the transition state of CH_3-CO_2 coupling on (a) Co(0001); (b) Ni(111); (c) Ru(0001); (d) Ir(111). The d states of the metals and 2p states of the O and C atoms are shown.

The electronic structure shows several common characteristics on the various metals. The p states of the C2 (C in the CO_2 moiety), O1, and O2 atoms hybridize in several sharp features between -6 and -8 eV below the Fermi level, which we identify as the molecular orbitals of the CO_2 moiety that partially retains its molecular identity at this stage of the reaction. These features also contain some contributions from the p states of the C1 atom (C in the methyl moiety), which is consistent with the fact that the C-C bond is in the process of being formed/broken. The highest concentration of the p states of C1 is, however, located between -5 and -6 eV. The p states of neither C atom show extensive interaction with the metal d states, whereas the p states of both O atoms do. Thus, the scaling of ΔE_{TS} for the C-C coupling step with ΔE_O has its origin in the extensive metal-oxygen electronic interactions. Incidentally, the adsorption energy of the product of the step, the acetate group, which preferentially adsorbs in a bidentate configuration via its O atoms on all the metals, also scales closely with ΔE_O with a slope of 0.5 [59].

3.3. Activation free energy analysis

As the adsorption of both CH_4 and CO_2 is weak on the metals, the entropic contents of CH_4 and CO_2 in gas phase can potentially have a significant impact on the respective steps. Therefore, in addition to the total-energy activation energies (E_a) reported above, we have also computed the

activation free energies (G_a) for the two steps. The results are plotted in Figure 5 as functions of temperature.

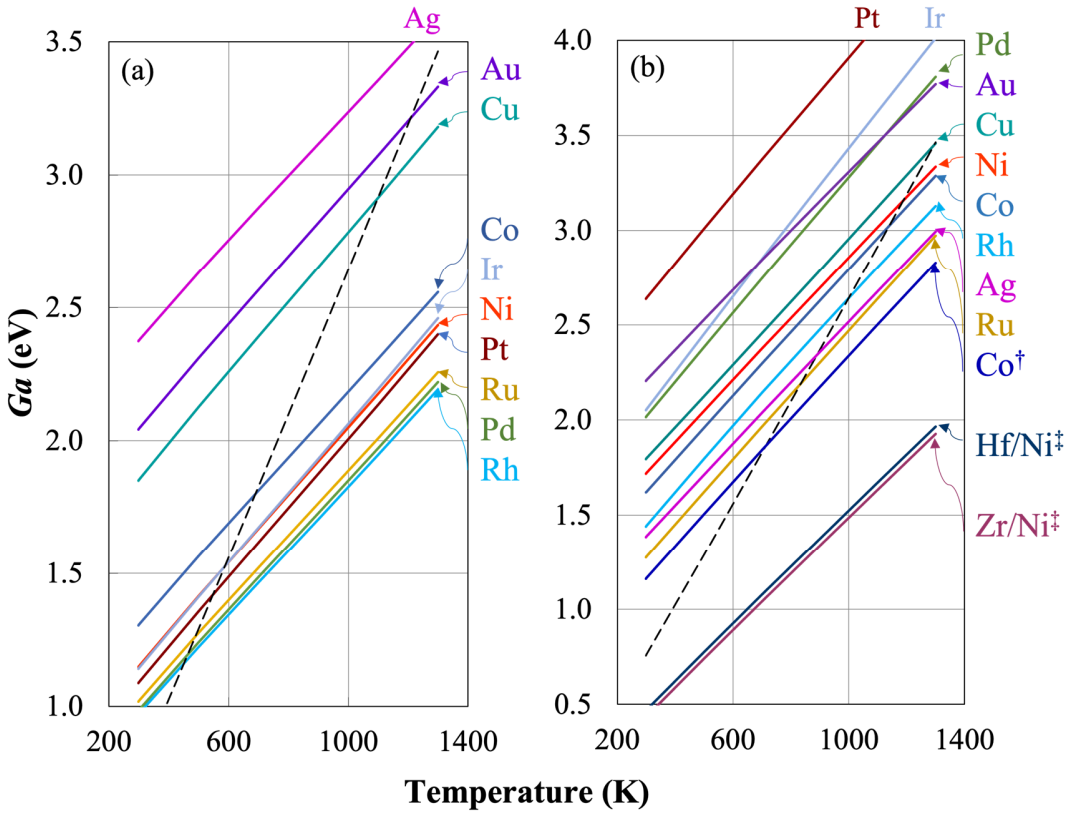

Figure 5. Activation free energy (G_a) for (a) initial C-H scission in CH_4 (with respect to gas-phase CH_4) and (b) CH_3-CO_2 coupling (with respect to adsorbed CH_3 and gas-phase CO_2), plotted as a function of temperature on the various metal surfaces. †, ‡ indicate CH-CO_2 coupling with respect to adsorbed CH and gas-phase CO_2 (‡ with co-adsorbed O). The dashed line represents G_a that yields a rate constant of 1 sec^{-1}·$site^{-1}$.

While the coinage metals are clearly poor catalysts for activating CH_4, the late 4d transition metals (Rh(111), Pd(111), and Ru(0001)) are the most active among the metals considered, followed by the late 5d and 3d transition metals (Figure 5a). Using a rate constant of

1 $sec^{-1}\cdot site^{-1}$ as criterion [60] (dashed lines in Figure 5), we estimate that Rh and Pd become reasonable catalysts for CH_4 dissociation at ca. 450 K, and Ru at 500 K. The corresponding temperature is ca. 550 K for Pt, 580 K for Ni, and 1100 K for Cu. These estimates are in line with available surface science evidence for CH_4 decomposition on transition metals. For instance, Stewart and Ehrlich reported that thermal excitation of gaseous CH_4 led to its dissociation on an Rh crystal held at 245 K [61]. Wu and Goodman exposed Ru(0001) to 5 torr of CH_4 for 120 seconds and observed the C-H bending mode of methylidyne (CH) in HREELS beginning at 400 K, which intensified at 500 K [62]. Schouten et al. reported no carbon deposition on Ni(111) under 10^{-2} torr of CH_4 for up to 5 hours at 523~618 K [63]. Bisson et al. showed Pt(111) to be more reactive than Ni(111) for dissociating CH_4 [64].

CH_3-CO_2 coupling is clearly more rate-limiting than CH_4 activation (Figure 5b). The estimated temperature required for this step is the lowest on Ru(0001), at 820 K, which would be problematic due to unwanted side reactions that would be permitted by the high temperature. The highly rate-limiting nature of this C-C coupling step prevents efficient formation of surface acetate species via MCC, which explains a lack of clear, reproducible evidence in the literature for acetate formation when CH_4 and CO_2 react on these metal surfaces.

To lower G_a for C-C coupling rests on a more stable TS. This could occur via 1) increase in CO_2 partial pressure, as we estimate that ca. 80% of the free energy contribution to G_a stems from the CO_2 moiety; 2) alternate CH_x-CO_2 coupling steps with $x < 3$; 3) catalyst modification. We will explore the latter two possibilities below.

3.4. Additional considerations

A common occurrence in catalytic conversion of hydrocarbons is successive C-H scissions that lead to strongly bound C_xH_y species on the catalyst surface. Steps generating CH_2, CH, and atomic C have different reaction energies on the different metals (Figure 6a). On Cu, Ag, and Au, all of the steps are endothermic making carbon formation and deposition thermodynamically highly unfavorable [32,43,51,65]. Of the remaining metals considered in this study, CH_3 decomposition is mildly endothermic on Co, Ni, Ir, and Pt, and CH is the most stable species on all of them, in line with existing theoretical literature [28,42,52,54,57]. Alloying with Au has been shown to alleviate coking of Ni reforming catalysts via destabilizing surface CH_x species and raising the CH_4 dissociation barrier [66], while adding small amounts of Ag to Ni can prevent ethylene dehydrogenation [67]. The coupling of surface CH_x species produces larger C_xH_y species [68–71], which eventually deactivates hydrocarbon-processing catalysts in the absence of an effective oxidizing or reducing agent [66,72]. Carbon buildup is a challenge not unique to MCC but is common to all manners of catalytic methane reforming.

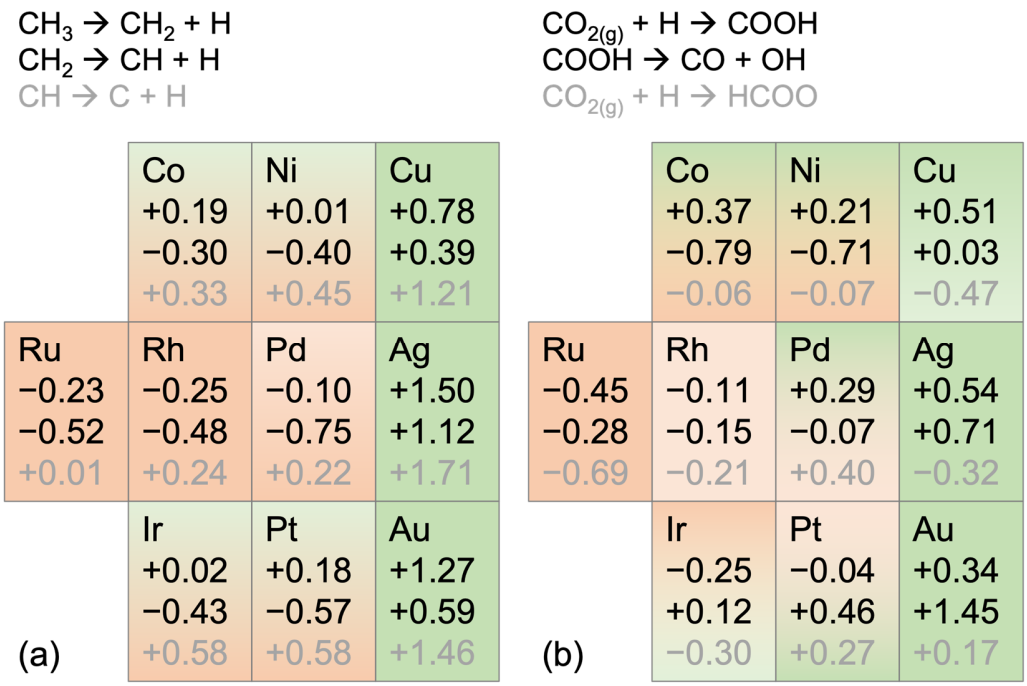

Figure 6. DFT-calculated reaction energies (ΔE_{rxn}) for (a) successive C-H scission steps starting from CH_3 and (b) CO_2 hydrogenation steps yielding various products (data adapted from Ref. [73]), on the close-packed (111) or (0001) surfaces of the ten catalytic metals considered in this study. Light/dark green/tan backgrounds indicate weak/strong endothermicity/exothermicity, respectively, for the first two steps of each reaction. The third step is not directly relevant to this study and is included for comparison.

While CH_4 dissociation needs to occur in MCC, CO_2 dissociation is not necessary but is possible. CO_2 dissociation can occur either directly on reactive metals to produce CO and O, or being assisted by atomic H to form carboxyl (COOH) that dissociates to produce CO and OH [74,75]. These can then be hydrogenated to C_1 oxygenates such as formaldehyde and methanol [76–78] and water, which are not the object of MCC. An ideal MCC catalyst should facilitate CH_x-CO_2 coupling but not CO_2 dissociation.

Herron et al. have reported DFT-calculated energetics for CO_2 hydrogenation to COOH on the close-packed (111) or (0001) surfaces of the metals considered in this study [73]. Their findings are summarized in Figure 6b. Among the metals considered in this study, CO_2 is least likely to be hydrogenated and dissociate into CO and OH on Cu, Ag, and Au. Hydrogenation to COOH is endothermic but further dissociation is exothermic on Co, Ni, and Pd. Exothermicity is reported for COOH formation on Ru, Rh, Ir and Pt (almost energetically neutral). Of the latter four, further dissociation into CO and OH is exothermic on Ru and Rh but endothermic on Ir and Pt. Incidentally, Cu, Ru, Rh, Ag, and Ir also favor formate (HCOO) formation [73], and the prevalence of HCOO on Cu is reflected in experimental observations, e.g., by Huang et al., that formic acid is a major side product in MCC on Cu-Co catalysts [8]. It should be noted that the COOH pathway is not solely a consequence of the catalyst metal but is also influenced by the reaction conditions, particularly the activity of hydrogen, which is controlled by the CH_4:CO_2 ratio and amounts of any additional hydrogen-yielding species present in the feed. A high hydrogen activity increases the likelihood of CO_2 dissociation via a hydrogen-assisted pathway.

Based on the reaction energy analysis above, we conclude that CH_3-CO_2 coupling is most relevant to MCC on the coinage metals; CH_3 and CH coupling to CO_2 on Co, Ni, and Pd; and CH_3 and CH coupling to COOH on Ir and Pt. Ru and Rh are too reactive to keep either reactant sufficiently intact to yield C_2 carboxylates. We present the parameters for the additional C-C coupling steps on the five metals with intermediate reactivity (Co, Ni, Pd, Ir, and Pt) in Table 3 (an extended list of CH_x-CO_2 coupling steps is presented in Table S1). The results suggest that C-C coupling via CH may provide a more accessible pathway to C_2 carboxylates than CH_3 on the five metals. The decrease in the C-C coupling barrier is negligible on Pd, and amounts to 0.2~0.6 eV on Co, Ni, Ir, and Pt. Hydrogenation of the resulting CHCOO species to acetate is

strongly exothermic. Except for Co(0001), where the CH pathway brings the rate of C-C coupling to a level comparable to that of CH_4 dissociation (Figure 5b), the alternate pathways do not ameliorate the rate-limiting nature of C-C coupling in MCC. The temperature required for Co(0001) to become a reasonable catalyst for MCC remains high (ca. 700 K, Figure 5a).

Table 3. GGA-PBE calculated activation barrier (E_a, in eV) and reaction energy (ΔE_{rxn}, in eV) for several additional C-C coupling steps in comparison to CH_3-CO_2 coupling from Table 2.

Surface	$CH_3 + CO_2$ → CH_3COO		$CH + CO_2$ → $CHCOO$		$CH_3 + COOH$ → $CH_3COO + H$		$CH + COOH$ → $CHCOO + H$		$CHCOO + 2H$ → CH_3COO
	E_a	ΔE_{rxn}	E_a	ΔE_{rxn}	E_a	ΔE_{rxn}	E_a	ΔE_{rxn}	ΔE_{rxn}
Co(0001)	1.12	-0.78	0.69	+0.15	-		-		-1.36
Ni(111)	1.22	-0.67	1.04	+0.51	-		-		-0.86
Pd(111)	1.52	-0.37	1.50	+1.03	-		-		-0.54
Ir(111)	1.51	-0.67	-		1.78	-0.44	1.23	+0.88	-0.91
Pt(111)	2.15	-0.04	-		1.91	-0.07	1.60	+1.09	-0.77

CO_2 is placed in the gas phase. Multiple intermediates in a given state are treated at infinite separation. The reaction energy for hydrogenation of CHCOO to CH_3COO (acetate) is included for comparison.

A major factor in CH_x-CO_2 coupling activity is the electronic stability of the TS. A possible strategy to enhance the CH_x-CO_2 coupling activity is therefore to enhance surface-oxygen interactions, thereby stabilizing the CO_2 moiety, with a single atom alloy (SAA) catalyst [79–83] based on a metal that is active for CH_4 dissociation (which rules out Cu, Ag, and Au) paired with a suitable oxophilic dopant. Such an SAA would possess separate sites for CH_4 activation and for CH_x-CO_2 coupling, the latter being more active than the host metal is, with

CH_x intermediates diffusing from the host sites to the dopant sites. For instance, Sykes and coworkers have shown recently that Ni and Pd sites in Ni-Au and Pd-Au SAAs are active for CH_3-CH_3 coupling [81,83]. Here we also rule out Pd and Pt because oxophilic early transition metal atoms prefer anti-segregation into the bulk of Pd and Pt as host metals, according to the surface segregation energies reported by Ruban et al. [84]. These considerations leave Co, Ni and Ir as potential host metals for the SAA approach.

Below we take Ni as example. Among early transition metals, Ruban et al. calculated that Zr and Hf strongly prefer to segregate to the Ni(111) surface [84]. Both metals are highly oxophilic, which can be seen in the heats of formation of the respective oxides (ZrO_2, -1097 kJ/mol [85]; HfO_2, -1118 kJ/mol [86]) and the fact that the dopant sites adsorb atomic O and acetate more strongly than monometallic Ni sites (Table 4). The energies of the TSs of the CH-CO_2 coupling steps on the Ni-based SAAs compared to Ni(111) are reported in Table 4, with the corresponding minimum-energy TS structures shown in Figure 6.

Table 4. Difference between GGA-PBE adsorption energy on representative Ni(111)-based SAA surfaces relative to same quantity on monometallic Ni(111) ($\Delta\Delta E$, in eV) for atomic C and O, acetate, TS of CH_4 activation (TS1), and TS of CH-CO_2 coupling (TS2).

Surface	$\Delta\Delta E_C$	$\Delta\Delta E_O$	$\Delta\Delta E_{acetate}$	$\Delta\Delta E_{TS1}$	$\Delta\Delta E_{TS2}$	$\Delta\Delta E_{TS2\text{-}O}$
Zr/Ni(111)	†	−0.72	−1.01	−0.15	−1.09	−1.04
Hf/Ni(111)	†	−0.76	−1.10	−0.15	−1.08	−1.00

†C avoids dopant sites. O is preferentially located on a threefold fcc site consisting of a dopant atom. Acetate is preferentially located on an adjacent pair of dopant-host top-top sites. TS2-O is TS2 with an O atom co-adsorbed on a threefold dopant site, with $\Delta\Delta E$ calculated relative to TS2 on clean Ni(111).

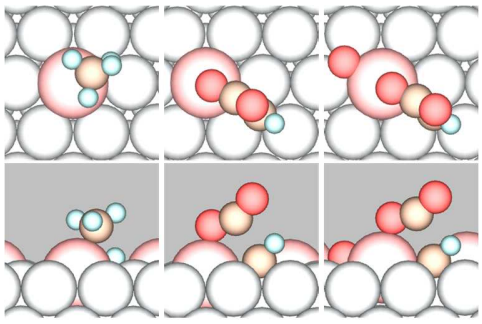

Figure 6. Top (top panels) and side (bottom panels) views of GGA-PBE optimized TS structures of (a) C-H scission, (b) CH-CO_2 coupling, and (c) CH-CO_2 coupling with a co-adsorbed O atom on Zr/Ni(111). The corresponding TSs on Hf/Ni(111) are shown in Figure S7. Color code: large spheres = metal; medium brown spheres = C; medium red spheres = O; small white spheres = H.

The results confirm that the dopant sites stabilize the TSs of C-C coupling relative to the host surfaces. The dopant metals do not significantly promote C-H scission in CH_4, but they clearly stabilize O-containing species including atomic O, acetate, and, in line with expectation, the TSs of CH_x-CO_2 coupling steps relative to monometallic Ni(111). Carboxy species, including CO_2, COOH, and acetate, could dissociate on such oxophilic sites to produce O or OH species that bind the dopant atoms preferentially and stabilize them in the host surfaces. The extent to which the formation of surface oxides is countered by atomic H from CH_4 dissociation depends on the metal species and hydrogen activity. Metals having highly exothermic heats of oxide formation, such as Zr and Hf, may remain oxidized under H_2-rich conditions. Promotional effect for C-C coupling is retained even when the dopant sites are partially oxidized (Table 4). Overall, Zr and Hf dopant sites in Ni(111) provide an electronic stabilization of ca. 1 eV to the TS of CH-CO_2 coupling (1.2 eV if compared to CH_3-CO_2 on Ni(111)), which significantly downshifts the Ni line in Figure 5b so that C-C coupling is no longer rate-limiting on Ni(111).

Ultimately, acetate is desired for coupling to another intermediate, such as an alkyne or CH_x, to form ester species. Depending on hydrogen activity, hydrogenated or dehydrogenated forms of acetate, including acetic acid and CHCOO, may also be involved. They allow for the possibility of an overall organic synthesis reaction with more favorable thermodynamics than MCC to acetic acid [16]. A lower reaction temperature, if made possible by SAA catalysts, helps reduce undesired side reactions and avoid worsening the thermodynamics for an overall reaction that combines multiple molecules into one. Whether the design strategy for alloy catalysts suggested here can successfully enable MCC to surface acetate formation remains to be verified experimentally.

4. Conclusions

Direct reactions between CO_2 and CH_4 have gained both research and industrial attention as potentially environmentally positive ways for chemical manufacture. However, both dry reforming and CH_4 carboxylation by CO_2 (MCC) to acetic acid are notably endergonic and require significant energy input. On the other hand, MCC to surface acetate followed by coupling to form esters provides the possibility of a thermodynamically more favorable overall reaction. It represents an appealing one-pot catalytic process that takes advantage of both CO_2 and CH_4 as abundant feedstock.

To explore the feasibility of this approach, we have performed periodic DFT calculations to investigate CH_4 activation and coupling to CO_2 forming surface acetate on ten late transition and coinage metal surfaces, including Co(0001), Ni(111), Cu(111), Ru(0001), Rh(111), Pd(111), Ag(111), Ir(111), Pt(111), and Au(111). The calculated DFT activation energy (E_a) for the initial C-H scission in CH_4 is ca. 1 eV or less on all the transition metals but considerably higher (> 1.5 eV) on the coinage metals. The E_a for CH_3-CO_2 coupling is 0.8 ~ 1.1 eV on Co, Ru, Rh, and Ag, 1.2 ~ 1.5 eV on Ni, Cu, Pd, and Ir, and 1.8 ~ 2.1 eV on Pt and Au. While the energy of the transition states (TSs) of the C-H scission in CH_4 scales the energy of atomic C (ΔE_C), that of the TSs of CH_3-CO_2 coupling scales closely with ΔE_O, not ΔE_C. This phenomenon occurs because metal-oxygen (as in CO_2) interactions play a dominant role in how the TSs of the second step adsorbs on the metal surfaces.

When free energy is taken into account, the CH_3-CO_2 coupling step is found to be much more rate-limiting than the initial CH_4 activation step. Overcoming it is predicted to require over 800 K even on the most active of the metals. Possible alternate C-C coupling steps involving CH_x (further dehydrogenated CH_4) and COOH (hydrogenated CO_2) are not sufficiently active to

ameliorate the rate-limiting nature of C-C coupling in MCC. Alternatively, based on the insight afforded by the electronic structure analysis, we propose that by doping an oxophilic metal into an active CH_4-activating surface to stabilize the transition state of CH_x-CO_2 coupling, one can create single atom alloy (SAA) catalysts that boost the C-C coupling activity compared to the host metals. Preliminary calculations on Zr and Hf-doped Ni(111) surfaces support this catalyst design strategy.

Acknowledgments

This work was supported by the U.S. Department of Energy, National Energy Technology Laboratory through NETL-Penn State University Coalition for Fossil Energy Research under Contract DE-FE0026825 and used high-performance computing resources provided by Louisiana State University.

References

[1] C. Song, Global challenges and strategies for control, conversion and utilization of CO_2 for sustainable development involving energy, catalysis, adsorption and chemical processing, Catal. Today. 115 (2006) 2–32. https://doi.org/10.1016/j.cattod.2006.02.029.

[2] A.P.E. York, T. Xiao, M.L.H. Green, Brief overview of the partial oxidation of methane to synthesis gas, Top. Catal. 22 (2003) 345–358. https://doi.org/10.1023/A:1023552709642.

[3] T. V. Choudhary, V.R. Choudhary, Energy-efficient syngas production through catalytic oxy-methane reforming reactions, Angew. Chemie - Int. Ed. 47 (2008) 1828–1847. https://doi.org/10.1002/anie.200701237.

[4] Russell D. Johnson III, NIST Computational Chemistry Comparison and Benchmark Database, NIST Standard Reference Database Number 101, 2020. https://doi.org/10.18434/T47C7Z.

[5] M.C.J. Bradford, M.A. Vannice, CO_2 reforming of CH_4, Catal. Rev. 41 (1999) 1–42. https://doi.org/10.1081/CR-100101948.

[6] S.C. Teuner, P. Neumann, F. Von Linde, CO through CO_2 reforming - The Calcor standard and Calcor economy processes, Oil Gas Eur. Mag. 27 (2001) 44–46.

[7] C. Tu, X. Nie, J.G. Chen, Insight into Acetic Acid Synthesis from the Reaction of CH4and CO2, ACS Catal. (2021) 3384–3401. https://doi.org/10.1021/acscatal.0c05492.

[8] W. Huang, K.-C. Xie, J.-P. Wang, Z.-H. Gao, L.-H. Yin, Q.-M. Zhu, Possibility of direct conversion of CH_4 and CO_2 to high-value products, J. Catal. 201 (2001) 100–104. https://doi.org/10.1006/jcat.2001.3223.

[9] W. Huang, C. Zhang, L. Yin, K. Xie, Direct synthesis of acetic acid from CH_4 and CO_2 in the presence of O_2 over a V_2O_5-$PdCl_2/Al_2O_3$ catalyst, J. Natual Gas Chem. 13 (2004) 113–

115.

[10] Y.-H. Ding, W. Huang, Y.-G. Wang, Direct synthesis of acetic acid from CH_4 and CO_2 by a step-wise route over Pd/SiO_2 and Rh/SiO_2 catalysts, Fuel Process. Technol. 88 (2007) 319–324. https://doi.org/10.1016/j.fuproc.2004.09.003.

[11] W. Huang, W.Z. Sun, F. Li, Efficient synthesis of ethanol and acetic acid from methane and carbon dioxide with a continuous, stepwise reactor, AIChE J. 70 (2009) NA-NA. https://doi.org/10.1002/aic.12073.

[12] A.M. Rabie, M.A. Betiha, S.E. Park, Direct synthesis of acetic acid by simultaneous co-activation of methane and CO_2 over Cu-exchanged ZSM-5 catalysts, Appl. Catal. B Environ. 215 (2017) 50–59. https://doi.org/10.1016/j.apcatb.2017.05.053.

[13] R. Shavi, J. Ko, A. Cho, J.W. Han, J.G. Seo, Mechanistic insight into the quantitative synthesis of acetic acid by direct conversion of CH_4 and CO_2: An experimental and theoretical approach, Appl. Catal. B Environ. 229 (2018) 237–248. https://doi.org/10.1016/j.apcatb.2018.01.058.

[14] E.M. Wilcox, G.W. Roberts, J.J. Spivey, Direct catalytic formation of acetic acid from CO_2 and methane, Catal. Today. 88 (2003) 83–90. https://doi.org/10.1016/j.cattod.2003.08.007.

[15] X. Nie, X. Ren, C. Tu, C. Song, X. Guo, J.G. Chen, Computational and experimental identification of strong synergy of the Fe/ZnO catalyst in promoting acetic acid synthesis from CH_4 and CO_2, Chem. Commun. 56 (2020) 3983–3986. https://doi.org/10.1039/C9CC10055E.

[16] J.J. Spivey, E.M. Wilcox, G.W. Roberts, Direct utilization of carbon dioxide in chemical synthesis: Vinyl acetate via methane carboxylation, Catal. Commun. 9 (2008) 685–689.

https://doi.org/10.1016/j.catcom.2007.08.023.

[17] Y. Zhao, C. Cui, J. Han, H. Wang, X. Zhu, Q. Ge, Direct C–C Coupling of CO_2 and the methyl group from CH_4 activation through facile insertion of CO_2 into Zn–CH_3 σ-bond, J. Am. Chem. Soc. 138 (2016) 10191–10198. https://doi.org/10.1021/jacs.6b04446.

[18] G. Kresse, J. Furthmüller, Efficient iterative schemes for ab initio total-energy calculations using a plane-wave basis set, Phys. Rev. B - Condens. Matter Mater. Phys. 54 (1996) 11169–11186. https://doi.org/10.1103/PhysRevB.54.11169.

[19] J.P. Perdew, K. Burke, M. Ernzerhof, Generalized gradient approximation made simple, Phys. Rev. Lett. 77 (1996) 3865–3868. https://doi.org/10.1103/PhysRevLett.77.3865.

[20] P.E. Blöchl, Projector augmented-wave method, Phys. Rev. B. 50 (1994) 17953–17979. https://doi.org/10.1103/PhysRevB.50.17953.

[21] G. Kresse, D. Joubert, From ultrasoft pseudopotentials to the projector augmented-wave method, Phys. Rev. B. 59 (1999) 1758–1775. https://doi.org/10.1103/PhysRevB.59.1758.

[22] M. Methfessel, A.T. Paxton, High-precision sampling for Brillouin-zone integration in metals, Phys. Rev. B. 40 (1989) 3616–3621. https://doi.org/10.1103/PhysRevB.40.3616.

[23] H.J. Monkhorst, J.D. Pack, Special points for Brillouin-zone integrations, Phys. Rev. B. 13 (1976) 5188–5192. https://doi.org/10.1103/PhysRevB.13.5188.

[24] G. Henkelman, H. Jónsson, A dimer method for finding saddle points on high dimensional potential surfaces using only first derivatives, J. Chem. Phys. 111 (1999) 7010–7022. https://doi.org/10.1063/1.480097.

[25] A. Hjorth Larsen, J. Jørgen Mortensen, J. Blomqvist, I.E. Castelli, R. Christensen, M. Dułak, J. Friis, M.N. Groves, B. Hammer, C. Hargus, E.D. Hermes, P.C. Jennings, P. Bjerre Jensen, J. Kermode, J.R. Kitchin, E. Leonhard Kolsbjerg, J. Kubal, K. Kaasbjerg, S.

Lysgaard, J. Bergmann Maronsson, T. Maxson, T. Olsen, L. Pastewka, A. Peterson, C. Rostgaard, J. Schiøtz, O. Schütt, M. Strange, K.S. Thygesen, T. Vegge, L. Vilhelmsen, M. Walter, Z. Zeng, K.W. Jacobsen, The atomic simulation environment—a Python library for working with atoms, J. Phys. Condens. Matter. 29 (2017) 273002. https://doi.org/10.1088/1361-648X/aa680e.

[26] P.L. Silvestrelli, A. Ambrosetti, Inclusion of screening effects in the van der Waals corrected DFT simulation of adsorption processes on metal surfaces, Phys. Rev. B. 87 (2013) 075401. https://doi.org/10.1103/PhysRevB.87.075401.

[27] N. Ferri, R.A. DiStasio, A. Ambrosetti, R. Car, A. Tkatchenko, Electronic properties of molecules and surfaces with a self-consistent interatomic van der Waals Density Functional, Phys. Rev. Lett. 114 (2015) 176802. https://doi.org/10.1103/PhysRevLett.114.176802.

[28] W. Huang, L. Sun, P. Han, J. Zhao, CH_4 dissociation on Co(0001): A density functional theory study, J. Nat. Gas Chem. 21 (2012) 98–103. https://doi.org/10.1016/S1003-9953(11)60339-3.

[29] Z. Zuo, W. Huang, P. Han, Z. Li, A density functional theory study of CH_4 dehydrogenation on Co(111), Appl. Surf. Sci. 256 (2010) 5929–5934. https://doi.org/10.1016/j.apsusc.2010.03.078.

[30] M. Mastromatteo, B. Jackson, The dissociative chemisorption of methane on Ni(100) and Ni(111): Classical and quantum studies based on the reaction path Hamiltonian, J. Chem. Phys. 139 (2013). https://doi.org/10.1063/1.4829678.

[31] A.P.J. Jansen, H. Burghgraef, MCTDH study of CH_4 dissociation on Ni(111), Surf. Sci. 344 (1995) 149–158. https://doi.org/10.1016/0039-6028(96)80003-3.

[32] X. Wang, Q. Yuan, J. Li, F. Ding, The transition metal surface dependent methane decomposition in graphene chemical vapor deposition growth, Nanoscale. 9 (2017) 11584–11589. https://doi.org/10.1039/C7NR02743E.

[33] K. Li, C. He, M. Jiao, Y. Wang, Z. Wu, A first-principles study on the role of hydrogen in early stage of graphene growth during the CH_4 dissociation on Cu(111) and Ni(111) surfaces, Carbon N. Y. 74 (2014) 255–265. https://doi.org/10.1016/j.carbon.2014.03.030.

[34] H. Mortensen, L. Diekhöner, A. Baurichter, A.C. Luntz, CH_4 dissociation on Ru(0001): A view from both sides of the barrier, J. Chem. Phys. 116 (2002) 5781–5794. https://doi.org/10.1063/1.1456509.

[35] A. Kokalj, N. Bonini, C. Sbraccia, S. de Gironcoli, S. Baroni, Engineering the reactivity of metal catalysts: A model study of methane dehydrogenation on Rh(111), J. Am. Chem. Soc. 126 (2004) 16732–16733. https://doi.org/10.1021/ja045169h.

[36] P.W. Van Grootel, R.A. Van Santen, E.J.M. Hensen, Methane dissociation on high and low indices Rh surfaces, J. Phys. Chem. C. 115 (2011) 13027–13034. https://doi.org/10.1021/jp2033774.

[37] Y.-H. (Cathy) Chin, C. Buda, M. Neurock, E. Iglesia, Consequences of metal–oxide interconversion for C–H bond activation during CH_4 reactions on Pd catalysts, J. Am. Chem. Soc. 135 (2013) 15425–15442. https://doi.org/10.1021/ja405004m.

[38] Q. Qi, X. Wang, L. Chen, B. Li, Methane dissociation on Pt(111), Ir(111) and PtIr(111) surface: A density functional theory study, Appl. Surf. Sci. 284 (2013) 784–791. https://doi.org/10.1016/j.apsusc.2013.08.008.

[39] B. Jackson, Direct and trapping-mediated pathways to dissociative chemisorption: CH_4 dissociation on Ir(111) with step defects, J. Chem. Phys. 153 (2020) 034704.

https://doi.org/10.1063/5.0012252.

[40] R. Zhang, L. Song, Y. Wang, Insight into the adsorption and dissociation of CH_4 on Pt(hkl) surfaces: A theoretical study, Appl. Surf. Sci. 258 (2012) 7154–7160. https://doi.org/10.1016/j.apsusc.2012.04.020.

[41] H. Guo, B. Jackson, Mode-selective chemistry on metal surfaces: The dissociative chemisorption of CH_4 on Pt(111), J. Chem. Phys. 144 (2016) 184709. https://doi.org/10.1063/1.4948941.

[42] H. Liu, R. Yan, R. Zhang, B. Wang, K. Xie, A DFT theoretical study of CH_4 dissociation on gold-alloyed Ni(111) surface, J. Nat. Gas Chem. 20 (2011) 611–617. https://doi.org/10.1016/S1003-9953(10)60252-6.

[43] W. Zhang, P. Wu, Z. Li, J. Yang, First-principles thermodynamics of graphene growth on Cu surfaces, J. Phys. Chem. C. 115 (2011) 17782–17787. https://doi.org/10.1021/jp2006827.

[44] C.F. Zinola, C. Gomis-Bas, G.L. Estiú, E.A. Castro, A.J. Arvia, A semiempirical quantum approach to the formation of carbon dioxide adsorbates on Pt(100) and Pt(111) cluster surfaces, Langmuir. 14 (1998) 3901–3908. https://doi.org/10.1021/la980447+.

[45] S.J. Choe, H.J. Kang, D.H. Park, D.S. Huh, J. Park, Adsorption and dissociation reaction of carbon dioxide on Ni(111) surface: Molecular orbital study, Appl. Surf. Sci. 181 (2001) 265–276. https://doi.org/10.1016/S0169-4332(01)00398-1.

[46] G.C. Wang, L. Jiang, Y. Morikawa, J. Nakamura, Z.S. Cai, Y.M. Pan, X.Z. Zhao, Cluster and periodic DFT calculations of adsorption and activation of CO_2 on the Cu(hkl) surfaces, Surf. Sci. 570 (2004) 205–217. https://doi.org/10.1016/j.susc.2004.08.001.

[47] S.G. Wang, X.Y. Liao, D.B. Cao, C.F. Huo, Y.W. Li, J. Wang, H. Jiao, Factors

controlling the interaction of CO_2 with transition metal surfaces, J. Phys. Chem. C. 111 (2007) 16934–16940. https://doi.org/10.1021/jp074570y.

[48] Y. Xu, R.B. Getman, W.A. Shelton, W.F. Schneider, A first-principles investigation of the effect of Pt cluster size on CO and NO oxidation intermediates and energetics, Phys. Chem. Chem. Phys. 10 (2008) 6009–6018. https://doi.org/10.1039/b805179h.

[49] S. Wang, V. Petzold, V. Tripkovic, J. Kleis, J.G. Howalt, E. Skúlason, E.M. Fernández, B. Hvolbæk, G. Jones, A. Toftelund, H. Falsig, M. Björketun, F. Studt, F. Abild-Pedersen, J. Rossmeisl, J.K. Nørskov, T. Bligaard, Universal transition state scaling relations for (de)hydrogenation over transition metals, Phys. Chem. Chem. Phys. 13 (2011) 20760–20765. https://doi.org/10.1039/c1cp20547a.

[50] F. Abild-Pedersen, J. Greeley, F. Studt, J. Rossmeisl, T.R. Munter, P.G. Moses, E. Skúlason, T. Bligaard, J.K. Nørskov, Scaling properties of adsorption energies for hydrogen-containing molecules on transition-metal surfaces, Phys. Rev. Lett. 99 (2007) 016105. https://doi.org/10.1103/PhysRevLett.99.016105.

[51] L. Xu, J. Lin, Y. Bai, M. Mavrikakis, Atomic and molecular adsorption on Cu(111), Top. Catal. 61 (2018) 736–750. https://doi.org/10.1007/s11244-018-0943-0.

[52] D.C. Ford, Y. Xu, M. Mavrikakis, Atomic and molecular adsorption on Pt(111), Surf. Sci. 587 (2005) 159–174. https://doi.org/10.1016/j.susc.2005.04.028.

[53] M. Neurock, W.T. Tysoe, Mechanistic insights in the catalytic synthesis of vinyl acetate on palladium and gold/palladium alloy surfaces, Top. Catal. 56 (2013) 1314–1332. https://doi.org/10.1007/s11244-013-0153-8.

[54] Y. Bai, D. Kirvassilis, L. Xu, M. Mavrikakis, Atomic and molecular adsorption on Ni(111), Surf. Sci. 679 (2019) 240–253. https://doi.org/10.1016/j.susc.2018.08.004.

[55] J.A. Herron, S. Tonelli, M. Mavrikakis, Atomic and molecular adsorption on Ru(0001), Surf. Sci. 614 (2013) 64–74. https://doi.org/10.1016/j.susc.2013.04.002.

[56] M. Mavrikakis, J. Rempel, J. Greeley, L.B. Hansen, J.K. Nørskov, Atomic and molecular adsorption on Rh(111), J. Chem. Phys. 117 (2002) 6737–6744. https://doi.org/10.1063/1.1507104.

[57] J.A. Herron, S. Tonelli, M. Mavrikakis, Atomic and molecular adsorption on Pd(111), Surf. Sci. 606 (2012) 1670–1679. https://doi.org/10.1016/j.susc.2012.07.003.

[58] W.P. Krekelberg, J. Greeley, M. Mavrikakis, Atomic and molecular adsorption on Ir(111), J. Phys. Chem. B. 108 (2004) 987–994. https://doi.org/10.1021/jp035786c.

[59] H. Olcay, L. Xu, Y. Xu, G.W. Huber, Aqueous-phase hydrogenation of acetic acid over transition metal catalysts, ChemCatChem. 2 (2010) 1420–1424. https://doi.org/10.1002/cctc.201000134.

[60] J.K. Nørskov, F. Studt, F. Abild-Pedersen, T. Bligaard, Fundamental Concepts in Heterogeneous Catalysis, Wiley, 2014. https://doi.org/10.1002/9781118892114.

[61] C.N. Stewart, G. Ehrlich, Dynamics of activated chemisorption: Methane on rhodium, J. Chem. Phys. 62 (1975) 4672–4682. https://doi.org/10.1063/1.430415.

[62] M.C. Wu, D.W. Goodman, High-resolution electron energy-loss studies of hydrocarbon formation from methane decomposition on Ru(0001) and Ru(1120) catalysts, J. Am. Chem. Soc. 116 (1994) 1364–1371. https://doi.org/10.1021/ja00083a023.

[63] F.C. Schouten, O.L.J. Gijzeman, G.A. Bootsma, Interaction of methane with Ni(111) and Ni(100); diffusion of carbon into nickel through the (100) surface; An aes-leed study, Surf. Sci. 87 (1979) 1–12. https://doi.org/10.1016/0039-6028(79)90164-X.

[64] R. Bisson, M. Sacchi, T.T. Dang, B. Yoder, P. Maroni, R.D. Beck, State-resolved

reactivity of CH_4 ($2\nu_3$) on Pt(111) and Ni(111): Effects of barrier height and transition state location, J. Phys. Chem. A. 111 (2007) 12679–12683. https://doi.org/10.1021/jp076082w.

[65] Y. Santiago-Rodríguez, J.A. Herron, M.C. Curet-Arana, M. Mavrikakis, Atomic and molecular adsorption on Au(111), Surf. Sci. 627 (2014) 57–69. https://doi.org/10.1016/j.susc.2014.04.012.

[66] F. Besenbacher, I. Chorkendorff, B.S. Clausen, B. Hammer, A.M. Molenbroek, J.K. Nørskov, I. Stensgaard, Design of a surface alloy catalyst for steam reforming, Science. 279 (1998) 1913–1915. https://doi.org/10.1126/science.279.5358.1913.

[67] R.T. Vang, K. Honkala, S. Dahl, E.K. Vestergaard, J. Schnadt, E. Lægsgaard, B.S. Clausen, J.K. Nørskov, F. Besenbacher, Controlling the catalytic bond-breaking selectivity of Ni surfaces by step blocking, Nat. Mater. 4 (2005) 160–162. https://doi.org/10.1038/nmat1311.

[68] M. Belgued, P. Pareja, A. Amariglio, H. Amariglio, Conversion of methane into higher hydrocarbons on platinum, Nature. 352 (1991) 789–790. https://doi.org/10.1038/352789a0.

[69] D. Howard Fairbrother, X.D. Peng, R. Viswanathan, P.C. Stair, M. Trenary, J. Fan, Carbon-carbon coupling of methyl groups on Pt(111), Surf. Sci. Lett. 285 (1993) L455–L460. https://doi.org/10.1016/0167-2584(93)90333-E.

[70] S. Chinta, T. V. Choudhary, L.L. Daemen, J. Eckert, D.W. Goodman, Characterization of C_2 (C_xH_y) intermediates from adsorption and decomposition of methane on supported metal catalysts by in situ INS vibrational spectroscopy, Angew. Chemie - Int. Ed. 41 (2002) 144–146. https://doi.org/10.1002/1521-3773(20020104)41:1<144::AID-ANIE144>3.0.CO;2-J.

[71] A.L. Marsh, K.A. Becraft, G.A. Somorjai, Methane dissociative adsorption on the Pt(111) surface over the 300-500 K temperature and 1-10 torr pressure ranges, J. Phys. Chem. B. 109 (2005) 13619–13622. https://doi.org/10.1021/jp051718+.

[72] A. Erdohelyi, J. Cserenyi, F. Solymosi, Activation of CH_4 and its reaction with CO_2 over supported Rh catalysts, J. Catal. 141 (1993) 287–299. https://doi.org/10.1006/jcat.1993.1136.

[73] J.A. Herron, J. Scaranto, P. Ferrin, S. Li, M. Mavrikakis, Trends in formic acid decomposition on model transition metal surfaces: A density functional theory study, ACS Catal. 4 (2014) 4434–4445. https://doi.org/10.1021/cs500737p.

[74] A.A. Gokhale, J.A. Dumesic, M. Mavrikakis, On the mechanism of low-temperature water gas shift reaction on copper, J. Am. Chem. Soc. 130 (2008) 1402–1414. https://doi.org/10.1021/ja0768237.

[75] L.C. Grabow, A.A. Gokhale, S.T. Evans, J.A. Dumesic, M. Mavrikakis, Mechanism of the water gas shift reaction on Pt: First principles, experiments, and microkinetic Modeling, J. Phys. Chem. C. 112 (2008) 4608–4617. https://doi.org/10.1021/jp7099702.

[76] A.A. Peterson, J.K. Nørskov, Activity descriptors for CO_2 electroreduction to methane on transition-metal catalysts, J. Phys. Chem. Lett. 3 (2012) 251–258. https://doi.org/10.1021/jz201461p.

[77] X. Nie, M.R. Esopi, M.J. Janik, A. Asthagiri, Selectivity of CO_2 reduction on copper electrodes: The role of the kinetics of elementary steps, Angew. Chemie Int. Ed. 52 (2013) 2459–2462. https://doi.org/10.1002/anie.201208320.

[78] S. Back, H. Kim, Y. Jung, Selective heterogeneous CO_2 electroreduction to methanol, ACS Catal. 5 (2015) 965–971. https://doi.org/10.1021/cs501600x.

[79] F.R. Lucci, T.J. Lawton, A. Pronschinske, E.C.H. Sykes, Atomic scale surface structure of Pt/Cu(111) surface alloys, J. Phys. Chem. C. 118 (2014) 3015–3022. https://doi.org/10.1021/jp405254z.

[80] M.D. Marcinkowski, M.T. Darby, J. Liu, J.M. Wimble, F.R. Lucci, S. Lee, A. Michaelides, M. Flytzani-Stephanopoulos, M. Stamatakis, E.C.H. Sykes, Pt/Cu single-atom alloys as coke-resistant catalysts for efficient C-H activation, Nat. Chem. 10 (2018) 325–332. https://doi.org/10.1038/NCHEM.2915.

[81] R. Réocreux, M. Uhlman, T. Thuening, P. Kress, R. Hannagan, M. Stamatakis, E.C.H. Sykes, Efficient and selective carbon-carbon coupling on coke-resistant PdAu single-atom alloys, Chem. Commun. 55 (2019) 15085–15088. https://doi.org/10.1039/c9cc07932g.

[82] R.T. Hannagan, G. Giannakakis, M. Flytzani-Stephanopoulos, E.C.H. Sykes, Single-Atom Alloy Catalysis, Chem. Rev. 120 (2020) 12044–12088. https://doi.org/10.1021/acs.chemrev.0c00078.

[83] P. Kress, R. Réocreux, R. Hannagan, T. Thuening, J.A. Boscoboinik, M. Stamatakis, E.C.H. Sykes, Mechanistic insights into carbon-carbon coupling on NiAu and PdAu single-atom alloys, J. Chem. Phys. 154 (2021). https://doi.org/10.1063/5.0048977.

[84] A. V. Ruban, H.L. Skriver, J.K. Nørskov, Surface segregation energies in transition-metal alloys, Phys. Rev. B. 59 (1999) 15990–16000. https://doi.org/10.1103/PhysRevB.59.15990.

[85] E. P.J. Linstrom and W.G. Mallard, NIST Chemistry WebBook, NIST Standard Reference Database Number 69, Natl. Inst. Stand. Technol. Gaithersbg. MD, 20899,. (2022). https://doi.org/https://doi.org/10.18434/T4D303.

[86] A.N. Kornilov, I.M. Ushakova, E.J. Huber, C.E. Holley, The enthalpy of formation of

hafnium dioxide, J. Chem. Thermodyn. 7 (1975) 21–26. https://doi.org/10.1016/0021-9614(75)90076-2.

$CH_4 + CO_2 \rightarrow$ acetate